

High-Energy Neutrino Flavor State Transition Probabilities

John Harrison^{1,2*}, Richard Anantua^{1,3}

1 Department of Physics and Astronomy, University of Texas at San Antonio, San Antonio, TX 78249, USA

2 Department of Mathematics and Statistics, Texas A&M University, Corpus Christi, TX 78412, USA

3 Department of Physics and Astronomy, Rice University, Houston, TX 77005, USA

*john.harrison@utsa.edu or john.harrison@tamucc.edu

Abstract

We analytically determine neutrino transitional probabilities and abundance ratios at various distances from the source of creation in several astrophysical contexts, including the Sun, supernovae and cosmic rays. In doing so, we determine the probability of a higher-order transition state from $\nu_\tau \rightarrow \nu_\lambda$, where ν_λ represents a more massive generation than Standard Model neutrinos. We first calculate an approximate cross section for high-energy neutrinos which allows us to formulate comparisons for the oscillation distances of solar, supernova and higher-energy cosmic ray neutrinos. The flavor distributions of the resulting neutrino populations from each source detected at Earth are then compared via fractional density charts.

Keywords: Neutrinos, Neutrino Oscillation, Detection

1 Introduction

As neutrinos oscillate along their path, their quantum mechanical wave packets develop phase shifts that change how they combine to produce a superposition of the three flavors ν_e , ν_μ and ν_τ . Thus, what starts as an electron neutrino may be detected in a detector as a muon or tau neutrino. On Earth, the electron neutrino, ν_e , is the most often detected. This makes sense as this state is what we would generally expect from Solar neutrinos [1].

Let us first recognize that the flavor states can accommodate an ultra-relativistic left-handed neutrino. We then allow this neutrino to have a flavor α ($\alpha = e, \mu, \tau$) and assume the neutrino to have a 4-momentum P^μ with spatial component, \vec{p} . Following [2], we write flavor states of the newly created neutrino

$$|\nu_\alpha\rangle = \sum_k U_{\alpha k}^* |\nu_k\rangle, \quad (1)$$

where $U_{\alpha k}$ is a unitary mixing matrix.

According to Giunti and Kim [2], observations show that our acquired state, $|\nu_k\rangle$, is a massive neutrino state, with its momentum \vec{p} as an eigenstate of the vacuum Hamiltonian, \mathcal{H}_0 , which can be written as

$$\mathcal{H}_0 |\nu_k\rangle = E_k |\nu_k\rangle \quad (2)$$

where, $E_k = \sqrt{p^2 + m_k^2}$

The total Hamiltonian in matter can then be written as

$$\mathcal{H} = \mathcal{H}_0 + \mathcal{H}_1 \quad (3)$$

where $\mathcal{H}_1 |\nu_\alpha\rangle = V_\alpha |\nu_\alpha\rangle$ [2]. This tells us that our effective potential from our initial neutrino, ν_α , is then described by the component, V_α [2]. We have seen that propagation of neutrinos is of quantum mechanical interest due to the phenomenon of state mixing; the production of neutrinos, on the other hand, garners appeal due to its implications for astrophysical environments.

The interior of a celestial body produces its own magnetic field through currents created by its rotation, which significantly influences the behavior of charged particles on the body's outer surface. When examining a star's collapse, it is essential to consider the acceleration of protons within the core of the collapsing star. This acceleration primarily results from the increasing pressure during the infall phases of the collapse. Additionally, cosmic rays, which are a characteristic of a planet's magnetosphere, may also contribute to the acceleration of particles from the core [3]. As part of this study, we investigate the potential generation of neutrinos from these cosmic rays.

Several elements contribute to understanding the acceleration of particles within a magnetosphere. This study focuses on a few of these elements, specifically the observation and analysis of distant cosmic rays, as well as first-order and second-order Fermi acceleration. Fermi acceleration describes the process by which a charged particle acquires energy due to shock speed or the movement of magnetic mirrors— with the order indicating how the energy gained relates to velocity. In the first-order process, magnetic fluctuations within shockwaves facilitate the acceleration. An example of first-order Fermi acceleration can be seen during a star's collapse, particularly during the bounce phase. Just before the material rebounds after collapsing inward, a shockwave is generated, aiding in the acceleration of charged particles within the magnetosphere itself [4]. Supernova remnant shocks serve as a significant astrophysical environment for first-order Fermi acceleration (diffusive shock acceleration) and are examined here as a potential site for neutrino production [3].

During second-order Fermi acceleration, stochastic acceleration by magnetic mirrors will have a role in answering each of our questions as well as playing a major part in the solution with regard to the probability of a complete flavor transformation. Magnetic mirrors assume the role of bouncing a particle back and forth accelerating it outward. The magnetic mirrors are in the form of a magnetic cloud pushing the charged particles along [4].

2 Neutrino Cross Sections

Since the first direct neutrino detection by Frederick Reines and Clyde Cowan in 1956 [5], neutrino cross sections have been notoriously small— concordant with the weakly interacting nature of neutrino interactions with matter. When considering the cross section as a product of energy gain, $\langle \frac{\Delta E}{E} \rangle = \frac{8}{3} (\frac{v}{c})^2$, we find the individual interaction cross sections estimated to range from $\sigma \equiv \sigma_{\nu_\mu - e \rightarrow \mu - \nu_e} \sim 1.33 \times 10^{-38} \text{cm}^2$ to $\sim 2.67 \times 10^{-38} \text{cm}^2$, where v is the speed of the magnetic cloud and c describes the speed of the particle [3].

In a lecture given at Fermilab in 2019 [6], it was shown that the simplest method for calculating cross sections relative to the event rate is by finding that

$$\frac{dN_r}{dt} = \sigma_r \cdot \frac{dN_f}{dt} \cdot n_b \cdot d \quad (4)$$

where, N_r is the number of reactions, $n_b \cdot d$ is the number of targets per surface unit with d being the individual target width. Here, N_f describes the number of particles within a beam [6] [7]. After integrating over t , we find

$$\sigma_r = \frac{N_r}{N_f} \frac{1}{n_b \cdot d} \quad (5)$$

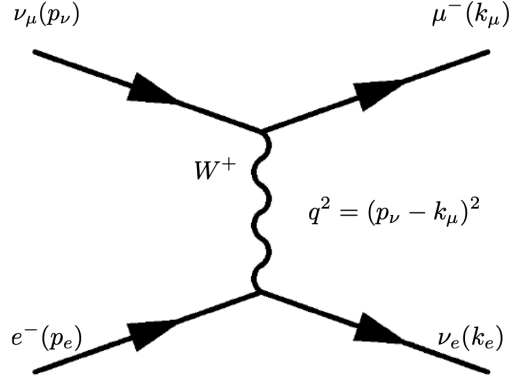


Figure 1. Feynman diagram depicting the scattering of an incoming muon-neutrino and an at rest electron. Figure used with permission of author [9].

The cross section for the interaction illustrated in Figure 1, in which a muon neutrino interacts with an electron to produce an electron neutrino and a muon, can be succinctly expressed as a function of neutrino energy by,

$$\sigma \approx \frac{2m_e G_F^2 E_\nu}{\pi} = \frac{G_F^2 s}{\pi} \quad (6)$$

However, to compute cross sections at high, or ultra-high energies such as that of cosmic rays, we have that

$$\frac{d\sigma(\nu_e)}{dy} = \frac{m_e G_F^2 E_\nu}{2\pi} ((g_V - g_A)^2 + (g_V - g_A^2)(1 - y)^2 - (g_V^2 - g_A^2)(\frac{m_e y}{E_\nu})) \quad (7)$$

where, $G_F = \frac{g^2}{4\sqrt{2}M_W^2} \approx 1.166 \times 10^{-5} \text{ GeV}^{-2}$, $y = 2m_e E_\nu$ which is the outgoing leptonic energy, bounded by $0 \leq y \leq y_{max} = 1 - \frac{m_l^2}{2m_e E_\nu + m_e^2}$. The coupling constants are given as $g_L = +1/2$, $g_R = 0$, $g_V = +1/2$ and $g_A = +1/2$ in which case L, R, V, A are the left, right, vector and axial components, respectively [9].

We can then determine approximate cross sections for high and ultra high energy cosmic rays. First, by substituting in our components $m_e = 9.11 \times 10^{-31} \text{ kg}$, with an energy of 300 GeV we obtain a value for y of $\sim 5.466 \times 10^{-28}$ which gives an approximate cross section of $5.072 \times 10^{-34} \text{ cm}^2$. Next, we can compare that with an energy level of 500 GeV or 0.5 TeV. This gives us a y value of $\sim 9.11 \times 10^{-28}$ in which we deduce a cross section of approximately $8.453 \times 10^{-34} \text{ cm}^2$. Lastly we will use an

energy of $E_\nu = 1,000$ GeV or 1 TeV, which is the energy level used in determining our cosmic ray probability calculations. The component y we find to be on the order of $\sim 1.822 \times 10^{-27}$. This yields an approximate neutrino cross section for cosmic rays as approximately 1.691×10^{-33} cm².

3 Oscillation and the Mean Free Path

Using the conversion probability function, we can ascertain the travel distance for oscillation and anticipate the state of our neutrino at a specific position and time. To simplify this process, it helps to conceptualize oscillating neutrinos as wave packets existing in some arbitrary state, $|\psi\rangle$. This arbitrary state is our initial condition in which we have $|\psi_\alpha\rangle$ where, α is the flavor eigenstate pre-measurement (or detection), $|\nu_e, \nu_\mu, \nu_\tau\rangle$. Similarly, $|\psi'_\alpha\rangle$ is our final state after detection. We must also consider the probability of measurement of the mass eigenstate. For the sake of simplification, we use the definition for neutrino flavor states as explained by Blasone, et al. (2022) [10], and utilizing the 3×3 Pontecorvo-Maki-Nakagawa-Sakata [PMNS] unitary mixing matrix [11], $\mathbf{U}(\tilde{\theta}, \delta)$, as follows:

$$|\underline{\nu}^{(f)}\rangle = \mathbf{U}(\tilde{\theta}, \delta) |\underline{\nu}^{(m)}\rangle \quad (8)$$

It is imperative to note, that in the above equation, we must explicitly show that there are two possible eigenstates: $|\underline{\nu}^{(f)}\rangle$ is our flavor eigenstate representing the transpose of $(|\nu_e\rangle, |\nu_\mu\rangle, |\nu_\tau\rangle)$. Then we have that $|\underline{\nu}^{(m)}\rangle$ is our mass eigenstate, which is represented by the transpose of $(|\nu_1\rangle, |\nu_2\rangle, |\nu_3\rangle)$. The probability for the flavor transition $\nu_\alpha \rightarrow \nu_\beta$ [2] can be defined as

$$P_{\nu_\alpha \rightarrow \nu_\beta}(t) = |\langle \nu_\beta | \nu_\alpha(t) \rangle|^2 = |\tilde{\mathbf{U}}_{\alpha\beta}(t)|^2 \quad (9)$$

This indicates the flavor transition at time, $t = 0$ with the contribution from [10]. Here we can assume from earlier that our variables, α and β , can represent any of the flavors (e, μ, τ) and we have that $\tilde{\mathbf{U}}(t = 0)$ is normalized [10].

We know from above that our neutrino flavor mixing matrix can be written as

$$\begin{pmatrix} \nu_e \\ \nu_\mu \end{pmatrix} = \begin{pmatrix} \cos \theta & \sin \theta \\ -\sin \theta & \cos \theta \end{pmatrix} \begin{pmatrix} \nu_1 \\ \nu_2 \end{pmatrix} \quad (10)$$

We can now show this as a unitary mixing matrix

$$\mathbf{U}(\theta) = \begin{pmatrix} \cos \theta & \sin \theta \\ -\sin \theta & \cos \theta \end{pmatrix} \quad (11)$$

Assuming that neutrinos have the ability to oscillate into three, four, or even an infinite number of flavors, we can illustrate the mixing phenomenon by examining a state involving two flavors. It is important to note that in the previous discussion, neutrinos were regarded as flavor states rather than as a combination of mass eigenstates, ν_1, ν_2, ν_3 . With this in mind, we can consider two weak eigenstates, ν_e and ν_μ . Their plane wave forms [2] can be expressed as

$$|\nu_1(t)\rangle = |\nu_1\rangle e^{i(\mathbf{p}_1 \cdot \mathbf{x} - E_1 t)} = |\nu_1\rangle e^{-ip_1 \cdot x} \quad (12)$$

and also

$$|\nu_2(t)\rangle = |\nu_2\rangle e^{i(\mathbf{p}_2 \cdot \mathbf{x} - E_2 t)} = |\nu_2\rangle e^{-ip_2 \cdot x} \quad (13)$$

If we let A be the flavor eigenstate consisting of e, μ, τ and let B be the neutrino mass eigenstate consisting of m_1, m_2, m_3 then we must consider that $A \times B \neq B \times A$. Assuming this constraint we can deduce that

$$A \times B = \{(e, m_1), (e, m_2), (e, m_3), (\mu, m_1), (\mu, m_2), (\mu, m_3), (\tau, m_1), (\tau, m_2), (\tau, m_3)\}.$$

Similarly,

$$B \times A = \{(m_1, e), (m_2, e), (m_3, e), (m_1, \mu), (m_2, \mu), (m_3, \mu), (m_1, \tau), (m_2, \tau), (m_3, \tau)\}.$$

Again we must stress the importance that for this assumption, the probability of A does not depend on the probability of B and the probability of B certainly does not depend on the probability of A . In other words, if we determine a state in A , that does not mean we know for certain state B , rather that all other probabilities for state B go to zero.

To consider the probability of an arbitrary neutrino state prediction, we must first consider a known constraint. To make a prediction based on a flavor eigenstate, we must assume that all mass eigenstate probabilities collapse. Conversely, if we are to make a prediction based on a mass eigenstate, all the flavor eigenstate probabilities collapse.

However, we must consider our neutrino eigenstates: $|\nu_e, \nu_\mu, \nu_\tau\rangle$ and $|m_1, m_2, m_3\rangle$. Because we are aware of our constraints, the same assumption made previously strictly applies here. That is the outcome observed for A does not depend on the outcome observed for B and the outcome observed for B does not depend on the outcome observed for A .

We can now determine the probability for flavor transition from $\nu_e \rightarrow \nu_\mu$ which corresponds to the detection of ν_e and is dependent on Δm as the mass difference, where, $\Delta m_{ij}^2 = m_i^2 - m_j^2$, E as the neutrino energy and the distance from the source, L .

$$P(\nu_e \rightarrow \nu_\mu) = 1 - \sin^2(2\theta_{21})\sin^2\left(\frac{1.27\Delta m_{21}^2[eV]L[m]}{E[MeV]}\right) \quad (14)$$

Alternatively, we can show the probability of our mass eigenstate and the prediction of the flavor state remaining in ν_e . We will reserve component, λ , as an arbitrary flavor state. The constraint here, however, is certainty in one eigenstate negates certainty in the other [2].

For comparative purposes, on Earth, we can expect a solar neutrino flux on the order of $\sim 5.9 \times 10^{14} \text{ m}^{-2}$ with approximately 1.7×10^{38} neutrinos being emitted every second. Considering the Type II supernova, SN1987A, located in the Large Magellanic Cloud, which was first detected on February 23, 1987. During its luminosity peak, approximately 5.9×10^{19} neutrinos were detected on Earth per second with an average flux of approximately $1.3 \times 10^{14} \text{ m}^{-2}$. The distance d from SN1987A to Earth is $\sim 168,000$ light years [12].

4 Sterile Neutrinos

As we consider the neutrino's ability to oscillate among ν_e, ν_μ, ν_τ , it is theoretically possible to oscillate into a heavier fourth flavor, without undergoing further oscillations, provided that this flavor interacts solely through the gravitational force. Due to this property, this fourth flavor has received the name sterile neutrino. It is essential to recognize that the sterile neutrino functions independently from the three active flavors. When a neutrino is generated, it can be described as a superposition of the three active flavors, each associated with their respective masses, while the sterile neutrino remains excluded from this interaction. Like other neutrinos, the sterile neutrino is electrically neutral and possesses a half-integer spin. As noted, this type of neutrino is anticipated to be heavier than the three known flavors, with theoretical mass estimates ranging from 10 GeV and 1 eV [13].

When we consider the existence of a sterile neutrino, we must also consider the probability of it being categorized as a Majorana particle. A fermion is considered Majorana when it is found to be its own antiparticle. Typical fermions are categorized as Dirac fermions at low energies, with the exception of the neutrino. Dirac fermions do not possess their own antiparticles. At this point, which category the sterile neutrino fits is unknown. If sterile neutrinos are Majorana, when two sterile neutrinos collide, they would annihilate each other with an enormous amount of energy.

We classify these particles as fermions, i. e., with a half-integer spin. In the context of neutrinos, this means their spin may either be $1/2$ or $-1/2$ depending on the spin quantum number s quantifying direction of intrinsic rotation. Neutrinos are typically considered to be “left-handed” fermions, i.e., with Dirac spinor representations that can be expressed as projections by the left-handed projection operator $P_L = \frac{1-\gamma^5}{2}$. Moreover, the W^\pm bosons mediating weak interactions involving neutrinos only interact with left-handed particles. When considering sterile neutrinos, they are assumed to be “right-handed” fermions, thus confirming the existence of a positive-spin neutrino.

If we take the mass of one “hand,” multiplied by the other “hand” we would deduce a constant mass.

So we can show that:

$$(RightHandMass) \times (LeftHandMass) = Constant \quad (15)$$

Therefore, we can now assume that if we were to increase the mass of one hand, that is, left or right, the other hand must become smaller. This results in a process referred to as the “Seesaw Mechanism” [13]

$$M_{(\nu)} = \begin{pmatrix} \nu_L f & \nu y \\ \nu y & \nu_R f \end{pmatrix} \quad (16)$$

where, f directly corresponds to neutrinos of heavier mass, however, a mixture of f results in neutrinos of lighter mass [13]. This yields the mass eigenstate of

$$M_{(\nu)} = \begin{pmatrix} 0 & M_D \\ M_D & M_{NHL} \end{pmatrix} \quad (17)$$

in which the mass hierarchy can be shown as $M_\nu \gg M_D \gg M_{NHL}$, where M_ν is the neutrino mass, M_D is the mass of the corresponding deuteron and M_{NHL} represents the neutral-heavy lepton [13]. By the Seesaw Mechanism, this yields an approximate neutrino mass of

$$M_\nu = \frac{M_D^2}{M_{NHL}} \quad (18)$$

Once again, the Seesaw Mechanism shows that if these right-handed sterile neutrinos exist, they could in fact be categorized as Majorana, which could help explain the difficulty in detecting them. This mechanism gives us a matrix theorizing six neutrino fields, three of which would have masses < 1 eV while the other three would have masses > 1 eV. Unlike other fermions, these Majorana particles do not exhibit intrinsic electric or magnetic moments. Instead, they would possess toroidal moments in which the field of the solenoid is bent into a torus.

5 Methods

We have previously shown the high probability of detecting our neutrino to be in states, ν_e or ν_μ . To consider a higher flavor transition, we must first consider the transition from ν_μ to ν_τ whose probability can be shown as [2]

$$P(\nu_\mu \rightarrow \nu_\tau) = \sin^2(2\theta_{32}) \sin^2 \left(\frac{1.27\Delta m_{32}^2 [eV] L[m]}{E[MeV]} \right) \quad (19)$$

We now need to expand the PMNS matrix [11] to include a fourth flavor by considering that:

$$\begin{aligned} |m_{ee}|_{4\nu} &= |\Sigma|U_{ej}|^2 e^{i\phi_j} m_j = \\ &|c_{13}^2 c_{12}^2 c_{14}^2 m_1 + c_{13}^2 c_{12}^2 c_{14}^2 e^{i\alpha} m_2 \\ &+ s_{13}^2 c_{14}^2 e^{i\beta} m_3 + s_{14}^2 e^{i\gamma} m_4 \end{aligned} \quad (20)$$

$$\begin{aligned} m_{ee} &= |\Sigma|U_{ej}|^2 e^{i\phi_j} m_j = \\ &|c_{13}^2 c_{12}^2 c_{14}^2 m_1 + c_{13}^2 c_{12}^2 c_{14}^2 e^{i\alpha} \sqrt{m_1^2 + \Delta_{21}} \\ &+ s_{13}^2 c_{14}^2 e^{i\beta} \sqrt{m_1^2 + \Delta_{31}} + s_{14}^2 e^{i\gamma} \sqrt{m_1^2 + \Delta_{41}} \end{aligned} \quad (21)$$

$$\begin{pmatrix} \nu_e \\ \nu_\mu \\ \nu_\tau \\ \nu_\lambda \end{pmatrix} = \begin{pmatrix} U_{e1} & U_{e2} & U_{e3} & U_{e4} \\ U_{\mu 1} & U_{\mu 2} & U_{\mu 3} & U_{\mu 4} \\ U_{\tau 1} & U_{\tau 2} & U_{\tau 3} & U_{\tau 4} \\ U_{\lambda 1} & U_{\lambda 2} & U_{\lambda 3} & U_{\lambda 4} \end{pmatrix} \begin{pmatrix} \nu_1 \\ \nu_2 \\ \nu_3 \\ \nu_4 \end{pmatrix} \quad (22)$$

where $U = R_{34}R_{24}R_{14}R_{23}R_{13}R_{12}P$ and so that [11] ,

$$\begin{aligned} R_{14} &= \begin{pmatrix} c_{14} & 0 & 0 & -s_{14}e^{i\delta_{14}} \\ 0 & 1 & 0 & 0 \\ 0 & 0 & 1 & 0 \\ -s_{14}e^{i\delta_{14}} & 0 & 0 & c_{14} \end{pmatrix} \text{ and} \\ R_{34} &= \begin{pmatrix} 1 & 0 & 0 & 0 \\ 0 & 1 & 0 & 0 \\ 0 & 0 & c_{34} & s_{34} \\ 0 & 0 & -s_{34} & c_{34} \end{pmatrix} \end{aligned} \quad (23)$$

We can now define the probability for a higher-order transition as

$$P(\nu_\tau \rightarrow \nu_\lambda) = \sin^2(2\theta_{43}) \sin^2 \left(\frac{1.27\Delta m_{43}^2 [eV] L[m]}{E[MeV]} \right) \quad (24)$$

where, $L[m]$ is the distance from the source, $E[MeV]$ is the energy and Δm is the mass difference between the flavors during the oscillation. This indicates that the probability of finding a neutrino in the fourth flavor state should be equal to the probability of finding it in the third flavor state.

Taking what we know from our probability functions, Equations (12) and (19), we can now use this to determine the probability for an n^{th} flavor. If we assume an oscillation into a fourth flavor, the sterile neutrino, is probable, then we can assume an equal probability of continuous oscillation into n flavors. We can now determine the theoretical travel distance for oscillation from $\nu_e \rightarrow \nu_\mu$ by assuming our mixing angle θ to be ~ 0.846 , our $|\Delta m_{21}|^2$ to be approximately $7.4 \times 10^{-5} \text{ (eV/c}^2\text{)}^2$ and we can assume an approximate energy E of 10^8 eV assuming a supernova neutrino creation. We can show a travel distance of approximately 10^{21} m or around 105,700 light years, with a probability of ~ 1 or $\sim 100\%$ of the transition from electron neutrino, ν_e , to muon

neutrino, ν_μ . Given this amount of travel distance, the neutrino would have definitively transitioned from its electron state, to its muon state.

To ascertain the pattern of transitional probabilities, a Python 3.13 program was developed to compare transitions between three widely detected neutrino types: solar, supernova and cosmic rays. For our first simulation, the following parameters were used for solar neutrinos:

For the first flavor change we will use for our mixing angle, $\sin^2\theta \approx 0.846$ and a mass difference of $\Delta m_{21}^2 \approx 7.40 \times 10^{-5} \text{ eV}^2$. For our second flavor change, $\sin^2\theta \approx 0.92$ and $\Delta m_{32}^2 \approx 2.40 \times 10^{-3} \text{ eV}^2$. For our third flavor change, $\sin^2\theta \approx 0.994$ and $\Delta m_{43}^2 \approx 0.05 \text{ eV}^2$. With an adopted solar neutrino energy of $E[\text{MeV}] \approx 1 \text{ MeV}$.

6 Results

We are now in a position to use our expression for neutrino transitional probabilities to estimate the neutrino transition fractions (among 3 species) at various distances. First we turn to our most important neutrino source, the Sun. The transitional probabilities from $\nu_e \rightarrow \nu_\mu$ and $\nu_\mu \rightarrow \nu_\tau$ are shown in Table 1 for solar neutrinos.

Table 1. Oscillation probabilities from Solar neutrinos at various distances from the source of neutrino production.

Distance $L[m]$	$\mathbf{P}(\nu_e \rightarrow \nu_\mu)$	$\mathbf{P}(\nu_\mu \rightarrow \nu_\tau)$	$\mathbf{P}(\nu_\tau \rightarrow \nu_\lambda)$
10^5	0.999	0.004	0.464
10^{10}	0.172	0.691	0.479
10^{15}	0.041	0.304	0.528
10^{20}	0.449	0.650	0.457
10^{25}	0.677	0.202	0.570
10^{27}	0.612	0.591	0.218

For Table 2, we maintain the parameters used above and apply them to neutrinos detected from supernova events. We assume a median supernova neutrino energy level of $\sim 10 \text{ MeV}$.

Table 2. Oscillation probabilities from supernova neutrinos at various distances from the source of neutrino production.

Distance $L[m]$	$\mathbf{P}(\nu_e \rightarrow \nu_\mu)$	$\mathbf{P}(\nu_\mu \rightarrow \nu_\tau)$	$\mathbf{P}(\nu_\tau \rightarrow \nu_\lambda)$
10^5	0.358	0.602	0.140
10^{10}	0.548	0.919	0.399
10^{15}	0.205	0.268	0.041
10^{20}	0.220	0.692	0.792
10^{25}	0.868	0.117	0.355
10^{27}	0.595	0.117	0.822

Finally, in Table 3, we consider a significant increase in energy. This is partly due to the first- and second- order Fermi processes within the magnetized clouds accelerating the cosmic rays. With this in mind, and again utilizing our base parameters, we now have an increased cosmic ray energy of $\sim 1 \times 10^6 \text{ MeV}$.

From the above tables, we have shown the distance needed to oscillate from the first flavor to the second flavor, with a consistently high probability of transition. Once we move into the second, third, and n^{th} flavors, we become less certain about our flavor transition probabilities. From the above two tables, we can infer why this is the case. We can clearly see that our probabilities for the higher flavors ($\mu \rightarrow \tau, \tau \rightarrow \lambda$) are the lowest when the probability for the transition from the first to the second flavor ($e \rightarrow \mu$) is at its highest. For example, for a cosmic ray neutrino, using our transition from

Table 3. Oscillation probabilities from cosmic ray neutrinos at various distances from the source of neutrino production.

Distance $L[m]$	$\mathbf{P}(\nu_e \rightarrow \nu_\mu)$	$\mathbf{P}(\nu_\mu \rightarrow \nu_\tau)$	$\mathbf{P}(\nu_\tau \rightarrow \nu_\lambda)$
10^5	0.999	0.000	0.000
10^{10}	0.358	0.602	0.126
10^{15}	0.548	0.919	0.359
10^{20}	0.205	0.268	0.041
10^{25}	0.216	0.692	0.792
10^{27}	0.605	0.198	0.667

$\nu_\tau \rightarrow \nu_\lambda$ at distances 10^5 m and 10^{10} m we obtained probabilities of $\sim 0.00\%$ and $\sim 12.6\%$, respectively.

When comparing this with our probability from $\nu_e \rightarrow \nu_\mu$ at the same distances, we find a probability of 99.9% but a significant decrease to $\sim 35.8\%$ when $\nu_\mu \rightarrow \nu_\tau$ is $\sim 60.2\%$. However, in Tables 1 and 3 there are distances from which our first flavor transition is approximately equal to our third flavor transition. In the case of Solar neutrinos, at $L[m] \sim 10^{20}$ m the probabilities for first and third transitions are $\sim 44.9\%$ and $\sim 45.7\%$, respectively. For the case with cosmic rays, we have that at $L[m] \sim 10^{27}$ m our first transition is $\sim 60.5\%$ while our third transition is $\sim 66.7\%$.

If we consider our distance of travel to be on the order of 1 AU Unit (AU), we find that our probability would be ~ 0.261 for flavor oscillation into the second state and ~ 0.111 for higher-order flavor transitions. When we compare this to known detection rates, we find approximately $\frac{2}{3}$ of detected neutrinos from the Sun to be found in either ν_e or ν_μ flavor state, which is consistent with our findings in the range of $\sim 26.1\%$ found in the ν_e flavor state [14].

A similar assumption can be made for atmospheric neutrinos. As cosmic rays bombard the atmosphere of Earth, protons strike the nuclei of atoms within our atmosphere forming pions. These short-lived particles decay into muons which then leave behind an electron, anti-electron and a neutrino, the ν_μ . This flavor, according to Fermilab, make up approximately $\frac{2}{3}$ of the detected neutrinos on Earth leaving behind $\frac{1}{3}$ to be detected as ν_e [14]. When comparing this with our calculations, we find that with cosmic rays we expect at a distance of 1.5×10^{11} m, ~ 0.399 to be in flavor state ν_e , while we have ~ 0.813 to be in state, ν_μ .

Taking these transition probabilities into account, we can quickly see that from varying distances and probabilities, the neutrino oscillation of flavors is simply a cycle of probabilities. In other words, the flavor transition can start again depending on the distance traveled prior to detection. What makes this concept more intriguing is that it helps explain a possible reasoning behind only having certainty in one eigenstate and not in both. When we measure a neutrino in a flavor eigenstate, we can assume that, and as the tables above show, as it oscillates between flavors it becomes a combination of all possible masses $m_1, m_2, m_3, \dots, m_n$. When we consider the combination of mass matrices, this also helps to understand the cycle of flavor oscillations prior to detection.

If we are to assume that when we observe a neutrino in state A or $|\nu^f\rangle$ we have the probability for $|\nu_e, \nu_\mu, \nu_\tau, \nu_\lambda\rangle$ with state B or $|\nu^m\rangle$ for $|m_1, m_2, m_3, m_\lambda\rangle$. We can predict our condition to be approximately as observed ν_e to have state B of $|m_1, 0, 0, 0\rangle$, for ν_μ we find $|m_1, m_2, 0, 0\rangle$, for ν_τ we would show $|m_1, m_2, m_3, 0\rangle$ and for ν_λ , $|m_1, m_2, m_3, m_\lambda\rangle$. This shows that each potential flavor state can be thought of simply as a combination of all possible masses.

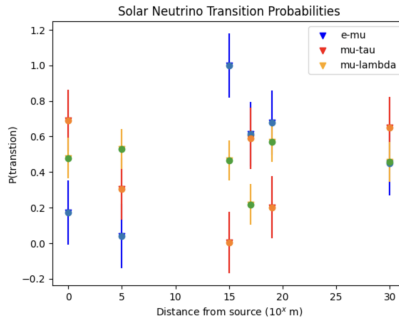


Figure 2. Scatter plot depicting the comparison of probabilities between solar neutrino flavor transitions $\nu_e \rightarrow \nu_\mu$, $\nu_\mu \rightarrow \nu_\tau$ and $\nu_\tau \rightarrow \nu_\lambda$.

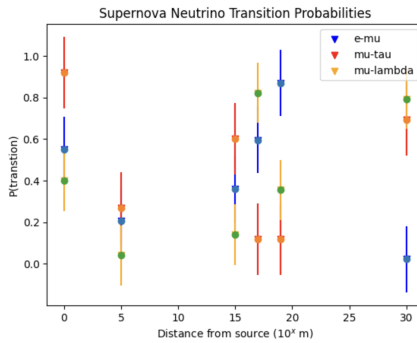


Figure 3. Scatter plot depicting the comparison of probabilities between supernova neutrino flavor transitions $\nu_e \rightarrow \nu_\mu$, $\nu_\mu \rightarrow \nu_\tau$ and $\nu_\tau \rightarrow \nu_\lambda$.

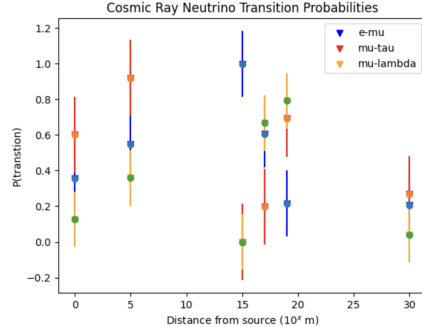


Figure 4. Scatter plot depicting the comparison of probabilities between cosmic ray flavor transitions $\nu_e \rightarrow \nu_\mu$, $\nu_\mu \rightarrow \nu_\tau$ and $\nu_\tau \rightarrow \nu_\lambda$.

7 Analysis of Results

In Figures 2-4, we show a comparison between the probabilities of the flavor transitions: $\nu_e \rightarrow \nu_\mu$, $\nu_\mu \rightarrow \nu_\tau$ and $\nu_\tau \rightarrow \nu_\lambda$ for solar, supernova and cosmic ray neutrinos, where λ is any higher order flavor transition from the $4^{th} \dots n^{th}$ flavor states. We can see from the probability distribution, that the closer we are to the source, the lower the probability of a higher-order flavor transition, as expected. However, as the neutrino oscillates at greater distances, a pattern of fluctuating probabilities can be observed. We can infer from this that as the neutrino approaches $\sim 10^{25}$ m from its source, the probabilities for all three flavors are all three approximations of each other, ± 0.10 . With this

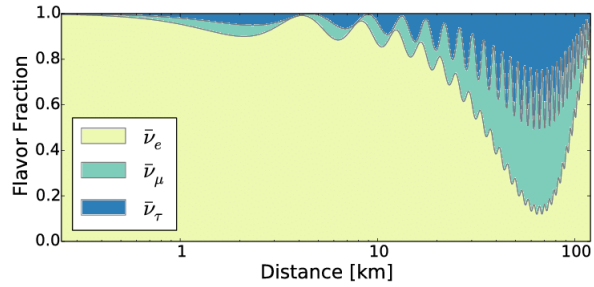


Figure 5. The above image shows the fraction of detected neutrino flavors with their corresponding oscillation distance. Figure used with permission of author [15].

understanding we can then follow the flavor transition by reverting backward through each flavor culminating at an equivalent point for both ν_e and ν_μ . From there, and as the neutrino oscillates further, we can then assume a probability for the first flavor as it approaches the probability for the n^{th} flavor transition; in this case, the sterile neutrino.

From the data in the figures above, we can ascertain that at a certain point, the probability of a neutrino oscillating into a fourth flavor state after a certain distance approaches the probability that the neutrino is being found in its first flavor state. This further shows that each flavor can be thought of as a proper combination of all mass and flavor eigenstates oscillating back and forth between states. The probability of oscillating into a higher n^{th} flavor is approximately the same as that of the neutrino oscillating backward through the previous states and beginning the cycle.

We can see in Figure 2, as the solar neutrino has traveled $\sim 10^{27}$ m from its source, the probability of it being found in the electron state is approximately the probability of it being found in its lambda state. From Figure 3, we can see the same equivalency; however with a supernova neutrino the distance is now $\sim 10^{20}$ m. With higher-energy neutrinos, such as those in Figure 4, we can see a unique symmetry between all three flavor of neutrino states. Here we can see where one flavor has a high probability, and the other two are at their lowest, and vice versa.

When we consider the neutrino's mean free path of $\sim 105,700$ light years, or 10^{21} m from its source, we can see that this fits perfectly with the neutrino energy stemming from supernova neutrinos. However, when we focus on the lower-energy solar neutrinos, we find that given a slightly further distance of travel (10^{27} m), we arrive at a near 0.5 probability of detecting our neutrino in the first and fourth flavor states. An inference here tells us that the lower-energy neutrinos, given a longer distance of oscillation, have a higher probability of oscillating back through and begins the cycle over again. higher-energy levels tend to oscillate much faster, creating a uniquely consistent probability distribution for flavor transformations.

From Figure 5, we can see the flavor fraction of detected neutrinos at the Reactor Experiment for Neutrino Oscillations (RENO) in South Korea [15]. When comparing this data to our above probabilities, and adjusting for unit of distance conversions, we find that for solar neutrinos at approximately 50 km we deduce a probability of $\nu_e \sim 0.985$, $\nu_\mu \sim 0.928$ and $\nu_\tau \sim 0.696$ and at 75 km $\nu_e \sim 0.473$, $\nu_\mu \sim 0.419$ and $\nu_\tau \sim 0.020$. In comparison with supernova neutrinos we find that at the same distances we have probabilities of $\nu_e \sim 0.202$, $\nu_\mu \sim 0.189$ and $\nu_\tau \sim 0.33$ and at 75 km $\nu_e \sim 0.473$, $\nu_\mu \sim 0.542$ and $\nu_\tau \sim 0.763$. Based on the above data, and our previous calculations the probability for cosmic ray neutrinos remain on the order of 10^{-5} until it reaches an approximate distance of $\sim 1 \times 10^5$ m or 100 km which is also shown in the above fraction distribution. These observations were conducted at RENO in South Korea. 2023 began new observations at JUNO in Guangdong, Southern China. Observations should be concluded Late 2024-Early 2025. It will be of great interest to note any similarities and/or differences in the observations.

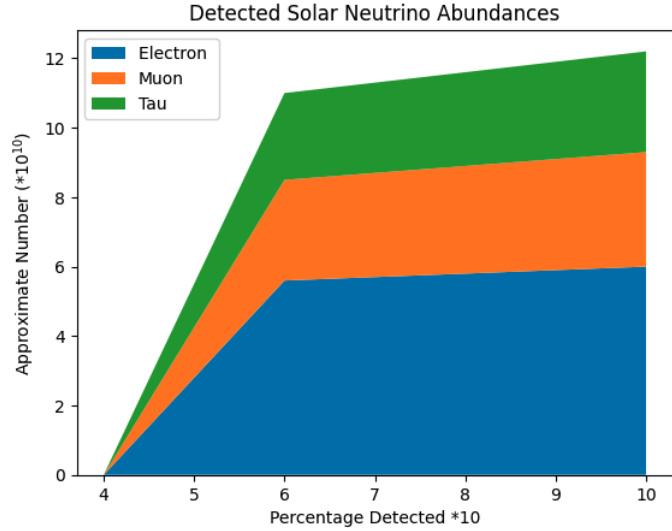


Figure 6. The above image shows the fraction of predicted solar neutrino flavor detection given an oscillation distance of 1.5×10^{11} m.

The density chart described in Figure 6 was calculated using a predicted flavor contribution to the solar neutrino flux detected on Earth. With an oscillation distance of $L_E = 1.5 \times 10^{11}$ meters, we find our changes to neutrino flavor abundance (number density) with distance for each observed flavor to be $\frac{\Delta}{\Delta L} \langle n_{\nu_e}, n_{\nu_\mu}, n_{\nu_\tau} \rangle \approx \langle n_0(1 - P_{12}), n_0 P_{12}(1 - P_{23}), n_0 P_{12} P_{23}(1 - P_{3\lambda}) \rangle$ where, n_0 is the original number density of electron neutrinos emitted from proton-proton chains within the Sun which is approximately 6.0×10^{10} cm² and P_{mn} are the corresponding flavor transition probabilities.

The neutrino flux can be found by $\frac{2L_{Sun}}{28MeV} \frac{1}{4\pi d^2} / \text{cm}^2 \approx 6.0 \times 10^{10}$ cm²s⁻¹. With an oscillation distance on the order of one AU, 10^{11} meters, we find the number of detected flavors we can expect on Earth from the Sun to be approximately 1.158×10^{11} neutrinos per square meter per second.

When comparing our probability density with the observed fraction density taken by RENO in South Korea [15], we can see that our predicted flavor detection at much greater distances, closely resembles those observed by RENO at a tenth of the distance from the Sun. This tells us that within distances of approximately 100,000 – 1,500,000 meters, our probabilities give us great confidence in our ability to predict flavor

transitions over great distances.

For comparative purposes, tables for both supernova neutrinos as well as those from cosmic rays were constructed using similar methods. However for the tables below, a supernova distance of 1.6×10^{21} m was used and for the cosmic rays a shorter distance of $\sim 10^{11}$ m was used for these particular densities.

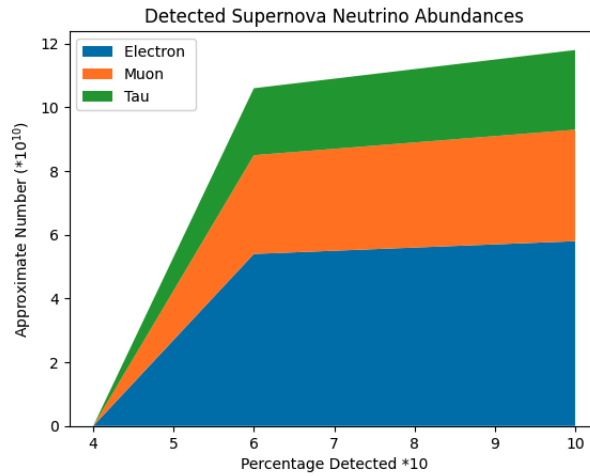


Figure 7. The above image shows the fraction of predicted supernova neutrino flavor detection given an oscillation distance of 1.6×10^{21} m.

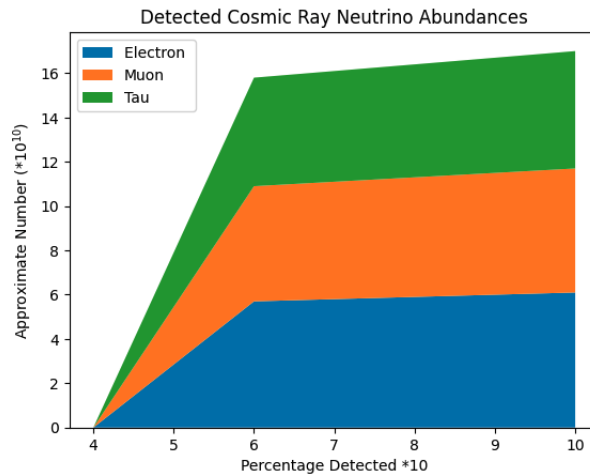


Figure 8. The above image shows the fraction of predicted cosmic ray neutrino flavor detection given an oscillation distance of $\sim 10^{11}$ m.

We found that for the supernova neutrinos, around 50% should be detected as electron neutrinos while $\sim 30\%$ to be detected as muon neutrinos and the final 20% should be detected as tau neutrinos. Interestingly for the cosmic ray neutrinos, we found that approximately 36% should be detected as electron neutrinos, 33% as muon neutrinos and 31% as tau neutrinos.

8 Discussion

In this paper we have shown that we can determine the probabilities of neutrino flavor states by first calculating the product of flavor eigenstate and then mass eigenstate probabilities. We found that the greater the distance from the source, the higher the probability of finding the neutrino in a different state than that in which it was produced. We found that for solar neutrinos, 10^5 m from the source, the neutrino has a 99.9% chance of being detected in the state, ν_μ , and a 46.4% chance of oscillating into a fourth flavor or simply reverting backwards. We find that at around 10^{27} m this process starts over again. For supernova neutrinos, we find that at the same distances, we expect to find ν_τ with a 60.2% chance and ν_e with a 35.8% chance. This time at around 10^{25} m we find the process starting again. For the higher-energy cosmic rays, we find a similarity between the probabilities of that and the solar neutrinos. When comparing at the same distances, we have 99.9% chance of detection in the state, ν_e and a 0.00% chance of higher flavor transitions. Again, back to our distance of 10^{27} m, we find the process starts again.

In repeating the same process, but for a distance of one AU unit, or 1.5×10^{11} m we found that our neutrino flux should be comprised of approximately 50% electron-neutrinos, 26.7% muon-neutrinos and 23% tau neutrinos. When we extend this distance a bit further for supernova we found approximately, 48%, 32% and 20% electron-, muon- and tau-neutrinos, respectively. When considering higher-energy cosmic rays at a distance of approximately 10^{11} m we found a surprising split between 36%, 33% and 31% for the electron-, muon- and tau-neutrinos. We have shown with minimal assumptions on well-established neutrino transition probability function that neutrino population statistics differ significantly among astrophysical sources. Both Solar and supernova neutrino populations detected on Earth are relatively ν_e -dominant, whereas higher-energy cosmic ray neutrinos that are candidates for Ice Cube, Super Kamiokande and future planned detectors have a relatively uniform flavor distribution.

So far, only three flavor states have been detected, however we have shown that the likelihood of oscillating into a fourth flavor is equal to the oscillation back through the previous flavors, $\nu_\tau \rightarrow \nu_\mu \rightarrow \nu_e$. This raises an important question: since we know the flavors are linear combinations of the mass eigenstates, is it possible for a fourth flavor transition or would the neutrino's transformation cease at the ν_τ and simply revert back to the first flavor state?

To put it more concisely, measuring in the flavor state prevents us from identifying the mass state, except as a linear combination of all possible masses. In future research, we may explore whether the assumption of non-locality suggests that mass eigenstates can also be represented as flavor eigenstates. We determined that when examining the probabilities of detected states, we can make predictions based on the distance traveled since their creation. We discovered that a neutrino not only has a nearly certain probability of oscillating further but also of oscillating back into earlier states. This opens up opportunities for further research to focus on mass eigenstates and investigate if combinations of masses can replicate other flavors, and vice versa.

Acknowledgements

The authors wish to thank Joseph A. Formaggio at MIT and Petr Vogel at Caltech for their permission to use Figure 1 and Figure 5, respectively.

References

1. BOREXINO Collaboration *Neutrinos from the primary proton-proton fusion process in the Sun*, *Nature*, vol. 512, no. 7515, pp. 383–386, 2014.

-
2. Giunti, C.; Kim, C. *Neutrino Physics and Astrophysics*, 1st ed., Publisher: Oxford University Press, United Kingdom, **2007**.
 3. Bustamente, M., Montoya, G.D.C. and Paula, W. and Chavez, J.A.D., et. al. *High-energy cosmic-ray acceleration, 2009 CERN-Latin-American School of High-Energy Physics, CLASHEP 2009 - Proceedings*, **533-539**, **2010**.
 4. Greco, A., et. al. *Stochastic Fermi acceleration in the magnetotail current sheet: A numerical study*, *Journal of Geophysical Research, Space Physics*, **2010**, **115**, **A2**
 5. Reines, F., Cowan, C.L. *Detection of the Free Neutrino*, *Phys. Rev., American Physical Society*, **1953**, **92**, **3**, **830-831**
 6. Fermilab and Rocco, N. Neutrino Cross sections. Available online:
https://indico.fnal.gov/event/19346/contributions/51548/attachments/32048/39314/Noemi_Rocco_Lepton_nucleus_cross_section_theory.pdf
(Accessed on 2/19/2024) **2019**
 7. Krauss, F. S Matrix and Cross Sections Simplified. Institute for Particle Physics Phenomenology, Department of Physics, University of Durham. Available online:https://www.ippp.dur.ac.uk/~krauss/Lectures/QuarksLeptons/Basics/S_Matrix.html (Accessed on 2/19/2024) **2019**
 8. Formaggio, J. A., Zeller, G.P. *From eV to EeV: Neutrino Cross-Sections Across Energy Scales*, **2013**, *arXiv:1305.7513v1 [hep-ph]*
 9. Formaggio, J. A., Zeller, G.P. *From eV to EeV: Neutrino Cross-Sections Across Energy Scales*, **2013**, *arXiv:1305.7513v1 [hep-ph]*
 10. Blasone, M.; De Siena, S.; Matrella, C. *Non-locality and entropic uncertainty relations in neutrino oscillations*. *Eur. Phys. J. Plus*, **2022**, **137**, 1272.
 11. Korana, B.S., Nautiyal, V.K. *Effective Neutrino Masses From Four Flavor Neutrino Mixing Matrix*, **2020**, *International Journal of Theoretical Physics*, **60**: 781-792.
 12. Page, D., et. al. *NS 1987A in SN 1987A*, *The Astrophysical Journal*, **2020**, **898**, 125.
 13. Akhmedov E.; Frigerio M. Duality in left-right symmetric seesaw mechanism. *Phys Rev Lett*. **2006**, *96*(6):061802.
 14. The Super-Kamiokande Collaboration *Atmospheric neutrino oscillation analysis with neutron tagging and an expanded fiducial volume in Super-Kamiokande I-V*, *Phys. Rev. D*, **109**, 072014, **2014**.
 15. Vogel, Petr; Wen, Liangjian; Zhang, Chao *Neutrino Oscillation Studies with Reactors* **2015** *Nature Communications* **6**. [10.1038/ncomms7935](https://doi.org/10.1038/ncomms7935)